Field Effect Modulation of Electrocatalytic Hydrogen Evolution at Back-Gated Two-Dimensional MoS_2 Electrodes

*Yan Wang[†,‡], Sagar Udyavara[‡], Matthew Neurock[‡] and, C. Daniel Frisbie[‡,]**

‡ Department of Chemical Engineering and Materials Science, University of Minnesota, 421 Washington Avenue SE, Minneapolis, Minnesota 55455, United States

† Department of Chemistry, University of Minnesota, 207 Pleasant Street SE, Minneapolis, Minnesota 55455, United States

ABSTRACT: Electrocatalytic activity for hydrogen evolution at monolayer MoS_2 electrodes can be enhanced by the application of an electric field normal to the electrode plane. The electric field is produced by a gate electrode lying underneath the MoS_2 and separated from it by a dielectric. Application of a voltage to the back-side gate electrode while sweeping the MoS_2 electrochemical potential in a conventional manner in 0.5 M H_2SO_4 results in up to a 140-mV reduction in overpotential for hydrogen evolution at current densities of 50 mA/cm^2. Tafel analysis indicates that the exchange current density is correspondingly improved by a factor of 4 to 0.1 mA/cm^2 as gate voltage is increased. Density functional theory calculations support a mechanism in which the higher hydrogen evolution activity is caused by gate-induced electronic charge on Mo metal centers adjacent the S vacancies (the active sites), leading to enhanced Mo-H bond strengths. Overall, our findings indicate that the back-gated working electrode architecture is a convenient and versatile platform for investigating the connection between tunable electronic charge at active sites and overpotential for electrocatalytic processes on ultrathin electrode materials.

KEYWORDS: electrocatalysis, hydrogen evolution reaction, MoS_2, field effect, gating, density functional theory

Previously, we have reported field effect modulation of outer-sphere electrochemistry at two-dimensional (2D) semiconductors,[1–3] such as monolayer MoS_2 and 5-nm-thick ZnO films grown by atomic layer deposition (ALD). In these experiments, the 2D material is supported on a dielectric such as SiO_2 with a backside gate electrode, forming a metal-oxide-semiconductor (MOS) heterostructure, as shown in Figure 1a. The backside gate may be a true metal electrode or, because of convenience, a heavily-doped Si substrate. Application of a back-gate voltage V_{BG} between the gate and an electrical contact to the 2D semiconductor simultaneously shifts the conduction and valence band edges and accumulates or depletes charge carriers in the semiconductor; this is the conventional field effect employed in silicon field effect transistors (MOSFETs).[4] In some sense this field effect modification of the 2D working electrode is akin to chemical doping in that the offset between the Fermi level (E_F) and the band edges is controllably changed (as in n-doping or p-doping). However, the field effect is distinctly different from chemical doping in that (1) it is electronically controlled, continuously variable, and easily reversible; (2) it is the band edges that shift in response to the field, not E_F, which means that the positions of these edges with respect to redox couples in solution are changed, which in turn implies that the heterogeneous electron transfer rate constants can be tuned.

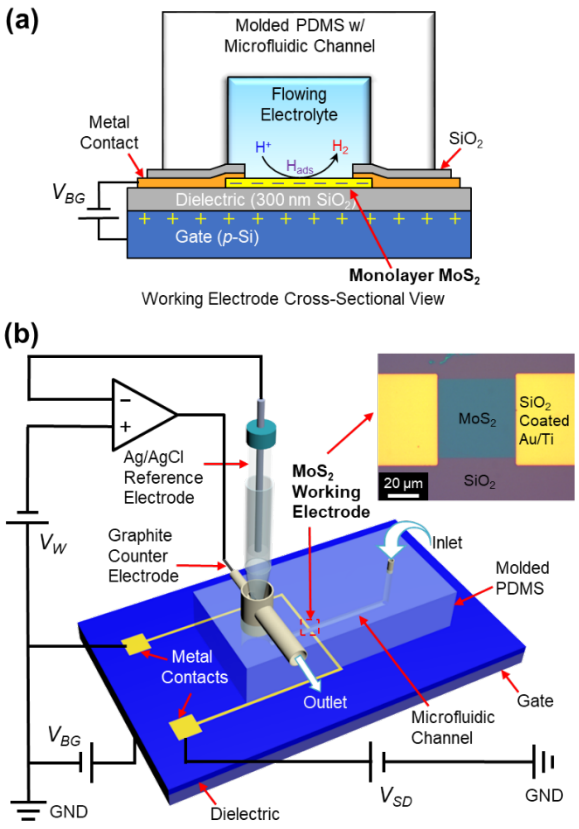

Figure 1. (a) Cross-sectional view of MoS_2 working electrode and (b) 3D structure of the back-gated electrochemical flow cell (not to scale) with the electrical/electrochemical configuration. The inset optical image in (b) shows a plan view of a MoS_2 electrode. The symbols used in the schematics are as follows: working electrode potential (V_W), source-to-drain bias (V_{SD}), and back-gate bias (V_{BG}).

We have shown that field effect modulation of the band edges and carrier concentration in monolayer MoS_2 and ultrathin ZnO can control heterogeneous charge transfer kinetics between the 2D material and simple, outer-sphere redox couples in electrolyte on the "front" side of the semiconductor. These initial experiments demonstrated the concept of field effect modulation of outer-sphere electrochemistry.[1–3] Here, we take the next step and demonstrate that field effect modulation can modify the rate of an inner-sphere, electrocatalytic reaction, namely the hydrogen

evolution reaction (HER) on MoS_2. Prior reports by others have demonstrated that both polymorphs of MoS_2 (metastable, metallic 1T and semiconducting 2H) are catalytically active for HER.[5–14] The activity of 2H MoS_2, our focus here, derives from coordinatively unsaturated Mo active sites, *i.e.*, Mo centers adjacent S vacancies or at exposed crystal edges. Consequently, S vacancy (active site) formation is a commonly adopted strategy to activate electrocatalysis on MoS_2,[7,15] though heteroatom doping is also employed.[16–18]

Prior to this work, the field effect has been reported to improve HER activity at back-gated *multilayer* MoS_2 electrodes.[19] However, in that work (see also a related paper on gated multilayer VSe_2[20]), the enhanced HER activity was attributed to increased conductivity of the multilayer MoS_2 (20-30 nm thick) upon gating and not to any changes in the intrinsic reactivity of the active sites. Herein, we demonstrate by a combination of experiment and density functional theory (DFT) calculations that field effect enhancement of HER activity on *monolayer* MoS_2 occurs by a different mechanism, namely the gate-induced charging of the localized Mo d-states at the active (S-vacancy) sites, and the resultant increase of the Mo-H binding energy. In this mechanism, the increase in HER activity is due to an increase in the intrinsic reactivity of the active sites in monolayer MoS_2 on applying a positive gate bias V_{BG}. Experimentally, we achieve a 140-mV decrease in η at 50 mA/cm^2 and a 4-fold increase in the exchange current density i_0 by varying V_{BG}. We systematically eliminate the possibility that the enhancement in i_0 and the decrease in η are due to changes in the MoS_2 conductivity or the resistance of the electrical contacts to MoS_2. Further, using DFT, we demonstrate that the charging of the Mo centers at the active sites leads to a 140% increase in the Mo-H bond energy, which provides a clear explanation for the enhanced HER activity. We believe these experiments and associated theoretical calculations open up new

possibilities for investigating and understanding electrocatalysis at 2D materials, as we describe below.

Monolayer MoS_2 was synthesized by chemical vapor deposition (CVD) at 850 ℃ following a modification of previously reported methods.[21,22] Large monolayer flakes that are desirable for back-gated electrocatalysis experiments were characterized by atomic force microscopy (AFM), Raman spectroscopy, and photoluminescence and confirmed the 2H phase (Figure S2). After the transfer of a monolayer of MoS_2 onto SiO_2/p-Si back gates, fabrication of MoS_2 electrodes was accomplished in a series of steps including photolithography, plasma etching, e-beam evaporation of Ti/Au metal contacts, and SiO_2 passivation (see the Supporting Information for details of synthesis and device fabrication). The two Ti/Au contacts (source and drain) were made to the front-side of MoS_2 and the completed structure in Figure 1a can thus be viewed as a FET. From the MoS_2 sheet conductance-gate voltage (G_S-V_{BG}) characteristics, Figure S6, we confirmed the n-type behavior of MoS_2 with an on/off current ratio of $\sim 10^4$ and a FET electron mobility of ~ 22 $cm^2\ V^{-1}s^{-1}$, which further confirmed that the monolayer MoS_2 was the 2H phase.

To perform electrochemical measurements, a molded polydimethylsiloxane (PDMS) block with an embedded 200-μm wide microfluidic channel was assembled onto a MoS_2 electrode, Figure 1b. Integration of this flow cell structure facilitated forced convection of electrolyte, thereby minimizing mass transport effects on voltammetry and helping to sweep away gas bubbles generated on the MoS_2 working electrode. Figure 2a displays our principal results, namely the polarization curves in flowing 0.5 M H_2SO_4 upon sweeping the MoS_2 working electrode potential V_W while applying a constant V_{BG}. At $V_{BG} = 0\ V$, the HER overpotentials ($\eta = |V_w - U^0|$) at current densities of 10 and 50 mA/cm^2 were 294 ± 11 and 478 ± 5 mV, respectively. These η values

at $V_{BG} = 0\ V$ are comparable to those previously reported for HER on monolayer MoS_2.[7,15,23,24] As V_{BG} increased from 0 V to +100 V at 20 V intervals, η progressively decreased to 176 ± 27 mV (at 10 mA/cm^2) and 334 ± 3 mV (at 50 mA/cm^2), respectively (Table 1), indicating an overall improved catalytic activity for HER. Negative V_{BG}, on the other hand, suppressed HER on back-gated MoS_2, resulting in an increased η. The effect of V_{BG} on HER activity was reversible, *i.e.*, switching of V_{BG} to higher and lower values produced corresponding voltammograms that retraced themselves. As a control, we tested back-gated working electrodes in which MoS_2 was replaced with graphene, Figure 2a. We observed no significant HER activity for back-gated graphene at any value of V_{BG} (Figure S9), consistent with expectations. We also verified that the observed shift in η was not a result of the ohmic drop across the MoS_2 working electrode. To check that, we measured the sheet resistance of MoS_2 electrodes simultaneously during the electrochemical measurement (Figure S8a). The calculated in-plane polarization at varying V_{BG} and V_W was always smaller than 11 mV (Figure S8b) and accounted for less than 1% of the overall polarization (*i.e.* η) at current densities of 10 and 50 mA/cm^2 (Figure S8c). Therefore, it is clear that the reduced η did not result from changes in the in-plane ohmic losses.

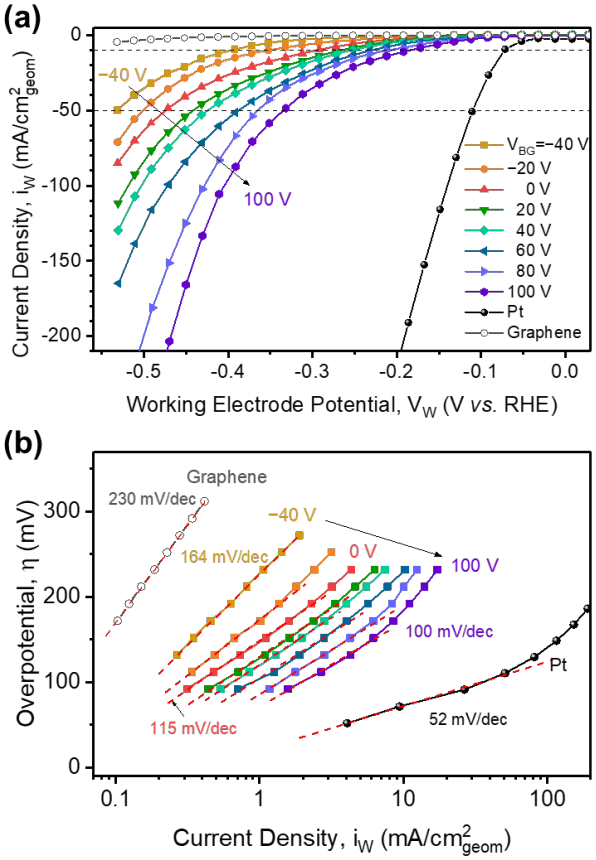

Figure 2. (a) Representative polarization curves and (b) corresponding Tafel plots for a back-gated MoS_2 electrode at different back-gate biases V_{BG} and in contact with 0.5 M H_2SO_4. Results on Pt and graphene electrodes are included for comparison. The polarization curves are iR-corrected for solution resistance. All the electrochemical measurements were performed at a working electrode potential scan rate of 50 mV/s and an electrolyte volumetric flow rate of 10 µL/min.

Table 1. Overpotential, Tafel Slope, and Exchange Current Density at Varying Back-Gate Biases

V_{BG} (V)	η at 10 mA/cm^2 (mV)	η at 50 mA/cm^2 (mV)	Tafel Slope* (mv/dec)	i_0 (mA/cm^2)
-40	388 ± 9	524 ± 8	164 ± 1	0.030 ± 0.001
-20	374 ± 20	500 ± 6	130 ± 4	0.032 ± 0.004
0	294 ± 11	478 ± 5	115 ± 2	0.034 ± 0.002
20	271 ± 8	451 ± 10	113 ± 3	0.047 ± 0.005
40	254 ± 9	421 ± 4	111 ± 3	0.054 ± 0.005
60	237 ± 7	390 ± 9	106 ± 6	0.068 ± 0.013
80	218 ± 11	371 ± 10	105 ± 4	0.098 ± 0.012
100	176 ± 27	334 ± 3	100 ± 6	0.122 ± 0.024

*The standard deviations for Tafel slope were calculated from fitting representative polarization curves to the Tafel equation.

The polarization curves in Figure 2a were converted into corresponding Tafel plots, Figure 2b, to assess the reaction mechanism. Tafel slopes (b) and exchange current densities (i_0) were obtained by fitting the plots to $\eta = b\,(\log(i_w) - \log(i_0))$. As expected, a Tafel slope of 115 ± 2 mV/decade is observed for HER on MoS_2 at V_{BG} = 0 V, consistent with ~120 mV/decade that others have reported for monolayer MoS_2 on Si/SiO_2.[9] The Tafel slope gradually decreases to 100 ± 6 mV/decade with increasing V_{BG}, while it increases to 164 mV/decade at negative V_{BG}. It is widely accepted that HER on MoS_2 follows the Volmer-Heyrovsky mechanism, where $H^+ + e^- \rightleftharpoons H_{ads}$ (Volmer) and $H^+ + e^- + H_{ads} \rightleftharpoons H_2$ (Heyrovsky) are the elementary steps.[25] Tafel slopes of ~120 mV/decade or larger suggest that the Volmer reaction, namely the coupled adsorption and charge transfer step, limits the overall reaction rate.[26] The slight decrease in the Tafel slope indicates that there is likely not a significant change in the reaction mechanism upon varying V_{BG}. However, the exchange density i_0 increases by a factor of 4 from 0.034 ± 0.002 to

0.122 ± 0.024 mA/cm^2 as V_{BG} increases to +100 V, as shown in Table 1 and Figure 3. These i_0 values obtained on back-gated MoS_2 are among the highest reported to date,[7–9,11] and the considerable increase in i_0 and suggests substantially enhanced catalytic activity at equilibrium. Figure 3 also shows the estimated turn over frequency per S vacancy (right axis) calculated from i_0 and average S vacancy concentration.

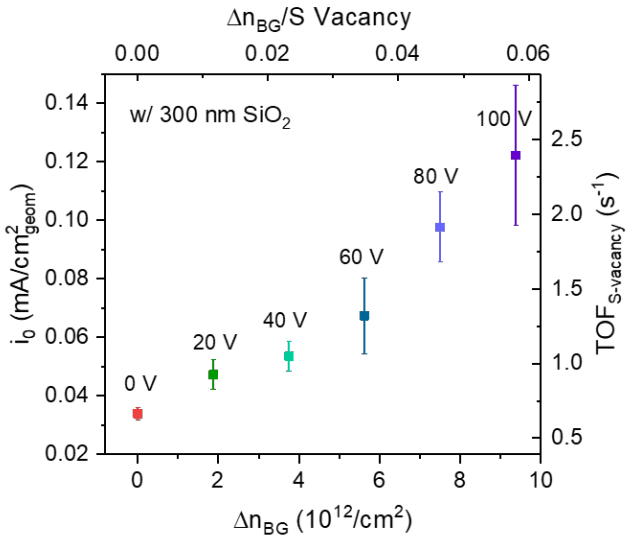

Figure 3. Exchange current density (i_0) and turn over frequency per S vacancy ($TOF_{S\text{-}vacancy}$) as a function of the back-gate induced charge carrier density, Δn_{BG}. The x-axis is quoted in electrons/cm^2 and electrons/S vacancy.

With more than a 100 mV shift in η at 10 mA/cm^2 and a 4-fold increase in i_0, it is reasonable to conclude that the overall HER activity of monolayer 2H MoS_2 is improved by the field effect. In order to clarify the mechanism for enhanced activity, DFT calculations were performed. The Mo centers adjacent to S vacancies on the MoS_2 basal plane are considered to be the active sites for HER.[7] X-ray photoelectron spectroscopy (XPS) analysis of the CVD monolayer MoS_2 used in this study indicated that there are ~7 ± 2% S vacancies (Figure S3) that function as

active sites. We therefore constructed a monolayer MoS_2 surface comprised of 5.5% S vacancies to serve as a model for DFT calculations, as shown in Figure 4a. The creation of S vacancies within the MoS_2 surface resulted in the formation of mid-gap electronic states (see Figure 4b and S10) comprised predominantly of localized Mo d-states that favorably bind protons.[7] To model the electrostatic doping effect of the back-gate bias on these mid-gap states, we charged the model substrate with extra electrons corresponding to the excess electron densities obtained experimentally (see Supporting Information for further details on the computational methods). Excess electron densities of nearly 1×10^{13} cm^{-2} as calculated by $\Delta n_{BG} = C_{SiO_2} \times V_{BG}$ (C_{SiO_2} is the specific capacitance of 300 nm SiO_2, measured to be ~15 nF/cm^2, Figure S10), are induced experimentally at V_{BG} = +100 V. Figure 4c displays the DFT-calculated electron density difference map corresponding to the difference in charge density at V_{BG} = +100 V (Δn_{BG} = 10^{13} cm^{-2}) versus that at 0 V (Δn_{BG} = 0). From this figure, it is evident that the excess electron density induced upon the application of V_{BG} is concentrated on the Mo atoms near the S vacancy site. This accumulation of excess electron density on the Mo centers in turn leads to a downward shift of the mid-gap states closer to E_F as V_{BG} is increased from 0 to +100 V as shown in Figure 4b. This downward shift of the energy levels is in agreement with expectations based on the known operating principles for field effect devices.

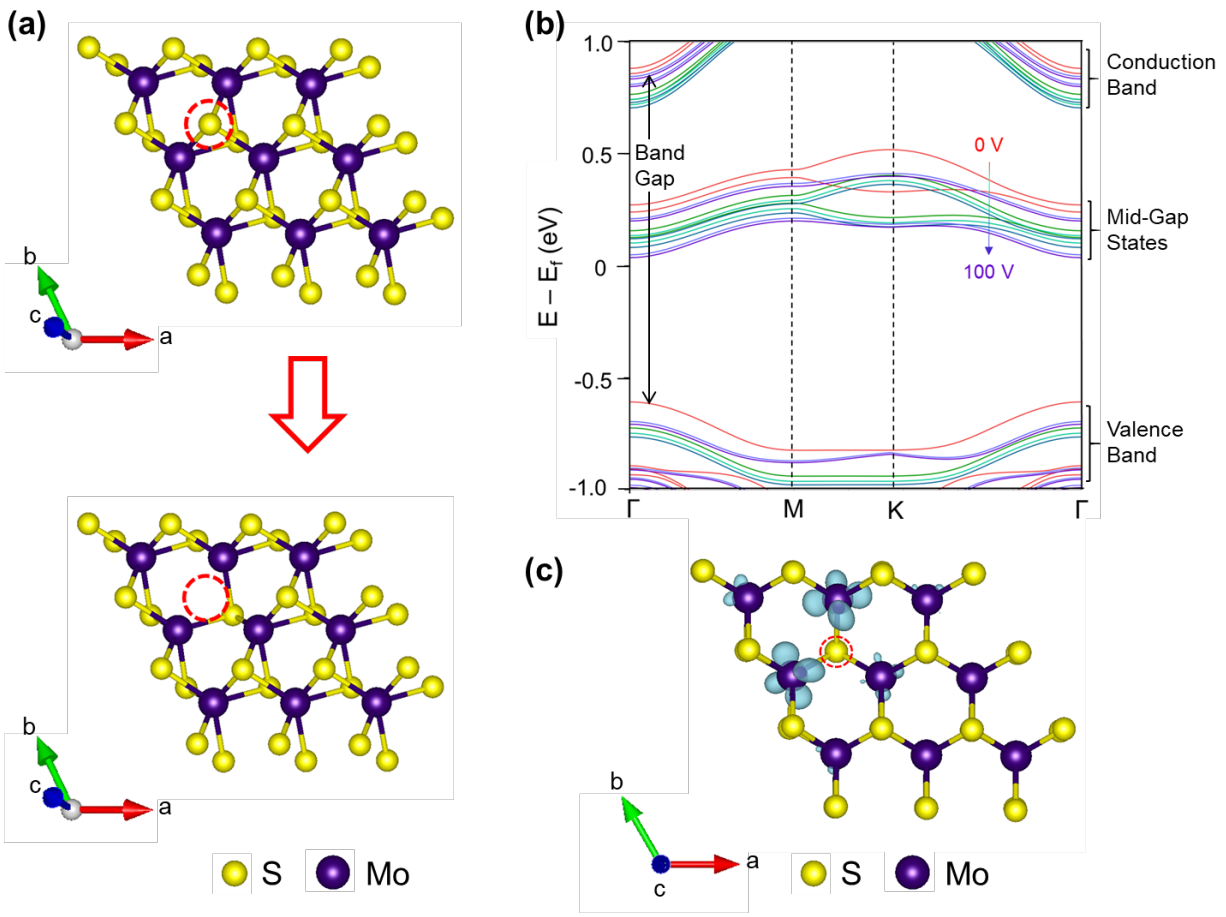

Figure 4. (a) Schematic of the S vacancy site (denoted by red dotted circle) created on model MoS_2 surface used for DFT calculations (b) Computed band structures of MoS_2 surface with 5.5 % S vacancy at different induced charges varying from $\Delta n_{BG} = 0$ ($V_{BG} = 0$ V) to $\Delta n_{BG} = 10^{13}$ cm^{-2} ($V_{BG} = 100$ V). The band structure at $V_{BG} = 0$ V is shown in red. (c) Charge density difference map (isosurface value = 0.0002 e-/Bohr^3) of monolayer MoS_2 with 5.5 % S vacancy showing the positive difference in electron density at an induced charge carrier density of 10^{13} cm^{-2} versus that at no excess charge density. The maps show localization of excess charge on the Mo atoms near the sulfur vacancy denoted by red circle.

The hydrogen adsorption free energy ($\Delta G_H = \Delta E_H + \Delta ZPE - T\Delta S$, where ΔE_H is the hydrogen adsorption energy, ΔZPE is the zero point energy difference, and ΔS is the entropy

change between the adsorbed and the gas phase hydrogen) to an electrode surface has been shown to be a good descriptor for trends in HER activity.[5] In the present study, the changes in ΔZPE and ΔS aren't expected to depend on charge. As such, we use ΔE_H to provide the important qualitative trends as described below. We calculated ΔE_H for the binding of hydrogen to the S vacancy site at charge densities corresponding to the applied back-gate voltages. As shown in Figure 5a, ΔE_H becomes significantly more exothermic at higher Δn_{BG}. Importantly, this stronger H binding provides a clear rationale for higher activity of adsorption-limited HER on MoS_2; increased ΔE_H lowers the activation energy for the Volmer step and leads to a higher fraction of hydrogenated active sites, *i.e.*, equilibrium is shifted in favor of H_{ads}.

In keeping with this analysis, we observed an exponential dependence of the experimental i_0 on the calculated ΔE_H values as shown in Figure 5b. This exponential increase is expected as i_0 is an exponential function of the activation barrier for the rate-limiting Volmer step.[27,28] The Figure 5b trend is also consistent with previous reports that show i_0 increases exponentially with ΔE_H for electrocatalysts that lie on the right side of the i_0 *vs.* ΔE_H "volcano plot", that is those that bind hydrogen weakly ($\Delta E_H > -0.2\ eV$).[5,28–30] Thus, the detailed DFT calculations reported here strongly support a mechanism in which the gate-induced charge enhances the intrinsic activity of the MoS_2 active sites, in particular by stabilizing H_{ads}.

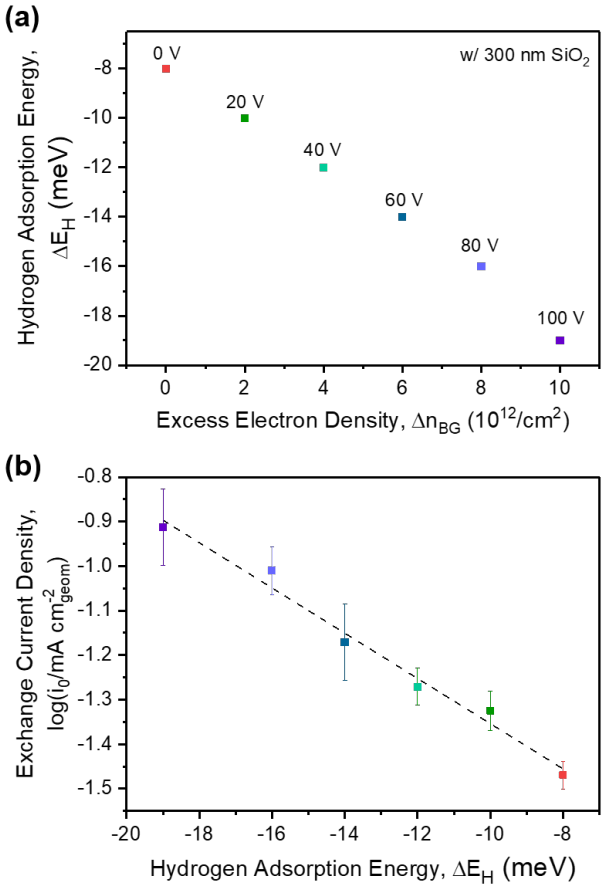

Figure 5. (a) Hydrogen adsorption energies (ΔE_H) as function of induced excess electron density (Δn_{BG}) for values ranging from 0 to 10^{13} cm^{-2} (b) Experimentally determined exchange current densities i_0 for hydrogen evolution on back-gated monolayer MoS_2 versus calculated ΔE_H.

The results reported here are distinctly different than previous work reported on field effect modulation of HER at multilayer (30-nm thick) MoS_2, which indicate that the decrease in η with applied gate voltage is the result of conductance changes across the MoS_2 flake, *i.e.*, to changes in the ohmic transport of charge from the contacts to the catalytic interface.[19] As mentioned above, using methods that we have previously reported[1] we categorically rule out the possibility that the changes in η are due to in-plane transport effects or to contact resistance.[9,19] The changes in η that we observe are instead due to changes in inherent catalytic activity of monolayer MoS_2. This is a

distinctly different mechanism from that proposed previously. Moreover, it does not seem likely that appreciable gate-induced enhancement of S-vacancy activity could be observed in 25-30 nm thick multilayer MoS_2 due to electrostatic confinement and screening of the gate-induced charge at the MoS_2/gate dielectric interface. For example, we estimate the Thomas-Fermi screening length in MoS_2 at $\Delta n_{BG} = 10^{13}$ cm^{-2} to be approximately 1-3 nm, smaller than the 25-30 nm thickness of multilayer MoS_2.

To our knowledge this is the first report of field-effect modulation to change the intrinsic activity of electrocatalytic sites on ultrathin, back-gated electrodes. To be clear, by "field-effect modulation" we mean the back-gating method we have employed here, not the normal double-layer charging that occurs in conventional electrochemical experiments. It is important to note that the back gate provides a degree of freedom that is not generally available in conventional electrocatalysis experiments. In a conventional electrocatalysis experiment, double-layer charging of active sites surely occurs but there is no ability to reversibly change the degree of charging independent of the electrochemical potential. With the back gate on sufficiently thin electrocatalyst layers, the amount of charge in the active sites is independently controlled and the impact on the overpotential can then be assessed directly and immediately, as demonstrated here.

There are other reports of electronic modification of gas-phase heterogeneous catalysts that have intriguing analogies to our experiments.[31,32] An example is the use of voltage-controlled Schottky junctions to manipulate electronic occupation in thin catalytic layers grown on doped semiconductors.[32] However, the use of an intervening dielectric in the platform we describe here can dramatically boost accumulated charge concentrations and provides flexibility in 2D electrode design as the alignment of the electrode band edges with the substrate is not a primary consideration.

The back-gated platform described here offers ample opportunities for further investigations of electrocatalysis at 2D electrodes for several reasons. First, the advent of ALD and 2D materials synthesis provides a rich palette of ultra-thin materials that can be coupled to gate/dielectric stacks and implemented as back-gated working electrodes. Second, the continuous, reversible electrostatic doping that is achieved in this platform can be a powerful complement to chemical (*e.g.*, heteroatom) doping strategies for optimizing 2D electrocatalysts. It will be interesting to understand in what ways electrostatic doping and chemical doping are similar or dissimilar. Third, as noted above, the independent control of electrode charging afforded by the back gate portends important opportunities to understand the differences in active site promotion by field-effect versus double-layer charging.

We note that the electrode architecture we have presented here is not fully optimized. For example, switching to high dielectric constant insulators, such as HfO_2, offers the possibility of simultaneously decreasing the required gate voltages and increasing the gate-induced carrier densities up to 10^{14} cm^{-2}. Preliminary computational results suggest a nearly 10-fold stronger hydrogen binding ($\Delta E_H = -146\, meV$) at such induced carrier densities, which should further enhance the utility of this platform for understanding HER (and other reactions) at ultrathin electrodes.

ASSOCIATED CONTENT

Supporting Information

Materials; synthesis of monolayer MoS_2; device fabrication; characterization: AFM image and Raman, photoluminescence, and XPS spectra of MoS_2; electrical and electrochemical measurements: sheet conductance of MoS_2 as a function of V_{BG} (without electrolyte), sheet resistance of MoS_2 measured in electrolyte simultaneously during electrochemical measurements,

calculated in-plane polarization of a MoS_2 electrode, polarization curves on a back-gated graphene electrode, determination of back-gate dielectric capacitance; computational methods.

The Supporting Information is available free of charge on the ACS Publications Website.

AUTHOR INFORMATION

Corresponding Author

*frisbie@umn.edu

Notes

The authors declare no competing financial interests.

ACKNOWLEDGMENT

The authors thank Dr. Chang-Hyun Kim for valuable discussions, Tony Whipple, Dr. Sushil Kumar Pandey and Dr. Youngdong Yoo for their help in the CVD synthesis, and Dr. Tao He, Dr. Zhuoran Zhang and Rui Ma for collecting AFM images. Y. W. acknowledges support through the Doctoral Dissertation Fellowship from the University of Minnesota. Parts of this work were carried out in the College of Science and Engineering Characterization Facility, University of Minnesota, which has received capital equipment funding from the NSF through the UMN MRSEC program under Award Number DMR-1420013, and in the Minnesota Nano Center which is supported by NSF through the National Nano Coordinated Infrastructure Network, Award Number NNCI - 1542202. We would also like to thank the MSI Supercomputing Institute at the University of Minnesota for use of its computing resources.

REFERENCES

(1) Kim, C.-H.; Frisbie, C. D. Field Effect Modulation of Outer-Sphere Electrochemistry at Back-Gated, Ultrathin ZnO Electrodes. *J. Am. Chem. Soc.* **2016**, *138* (23), 7220–7223.

(2) Wang, Y.; Kim, C.-H.; Yoo, Y.; Johns, J. E.; Frisbie, C. D. Field Effect Modulation of Heterogeneous Charge Transfer Kinetics at Back-Gated Two-Dimensional MoS_2 Electrodes. *Nano Lett.* **2017**, *17* (12), 7586–7592.

(3) Kim, C.-H.; Wang, Y.; Frisbie, C. D. Continuous and Reversible Tuning of Electrochemical Reaction Kinetics on Back-Gated 2D Semiconductor Electrodes: Steady-State Analysis Using a Hydrodynamic Method. *Anal. Chem.* **2019**, *91* (2), 1627–1635.

(4) Sze, S. M.; Ng, K. K. Physics of Semiconductor Devices. In *Physics of Semiconductor Devices*; John Wiley & Sons, Inc.: Hoboken, NJ, USA, 2006; pp 293–360.

(5) Jaramillo, T. F.; Jørgensen, K. P.; Bonde, J.; Nielsen, J. H.; Horch, S.; Chorkendorff, I. Identification of Active Edge Sites for Electrochemical H_2 Evolution from MoS_2 Nanocatalysts. *Science* **2007**, *317* (5834), 100–102.

(6) Hinnemann, B.; Moses, P. G.; Bonde, J.; Jørgensen, K. P.; Nielsen, J. H.; Horch, S.; Chorkendorff, I.; Nørskov, J. K. Biomimetic Hydrogen Evolution: MoS_2 Nanoparticles as Catalyst for Hydrogen Evolution. *J. Am. Chem. Soc.* **2005**, *127* (15), 5308–5309.

(7) Li, H.; Tsai, C.; Koh, A. L.; Cai, L.; Contryman, A. W.; Fragapane, A. H.; Zhao, J.; Han, H. S.; Manoharan, H. C.; Abild-Pedersen, F.; Nørskov, J. K.; Zheng, X. Activating and Optimizing MoS_2 Basal Planes for Hydrogen Evolution through the Formation of Strained Sulphur Vacancies. *Nat. Mater.* **2015**, *15*, 48.

(8) Li, G.; Zhang, D.; Qiao, Q.; Yu, Y.; Peterson, D.; Zafar, A.; Kumar, R.; Curtarolo, S.; Hunte, F.; Shannon, S.; Zhu, Y.; Yang, W.; Cao, L. All The Catalytic Active Sites of MoS_2 for Hydrogen Evolution. *J. Am. Chem. Soc.* **2016**, *138* (51), 16632–16638.

(9) Voiry, D.; Fullon, R.; Yang, J.; de Carvalho Castro e Silva, C.; Kappera, R.; Bozkurt, I.; Kaplan, D.; Lagos, M. J.; Batson, P. E.; Gupta, G.; Mohite, A. D.; Dong, L.; Er, D.; Shenoy, V.

B.; Asefa, T.; Chhowalla, M. The Role of Electronic Coupling between Substrate and 2D MoS_2 Nanosheets in Electrocatalytic Production of Hydrogen. *Nat. Mater.* **2016**, *15* (9), 1003–1009.

(10) Li, Y.; Wang, H.; Xie, L.; Liang, Y.; Hong, G.; Dai, H. MoS_2 Nanoparticles Grown on Graphene: An Advanced Catalyst for the Hydrogen Evolution Reaction. *J. Am. Chem. Soc.* **2011**, *133*, 7296.

(11) Wang, H.; Lu, Z.; Xu, S.; Kong, D.; Cha, J. J.; Zheng, G.; Hsu, P.-C.; Yan, K.; Bradshaw, D.; Prinz, F. B.; Cui, Y. Electrochemical Tuning of Vertically Aligned MoS_2 Nanofilms and Its Application in Improving Hydrogen Evolution Reaction. *Proc. Natl. Acad. Sci.* **2013**, *110* (49), 19701–19706.

(12) Voiry, D.; Salehi, M.; Silva, R.; Fujita, T.; Chen, M.; Asefa, T.; Shenoy, V. B.; Eda, G.; Chhowalla, M. Conducting MoS_2 Nanosheets as Catalysts for Hydrogen Evolution Reaction. *Nano Lett.* **2013**, *13* (12), 6222–6227.

(13) Lukowski, M. A.; Daniel, A. S.; Meng, F.; Forticaux, A.; Li, L.; Jin, S. Enhanced Hydrogen Evolution Catalysis from Chemically Exfoliated Metallic MoS_2 Nanosheets. *J. Am. Chem. Soc.* **2013**, *135* (28), 10274–10277.

(14) Wang, H.; Lu, Z.; Kong, D.; Sun, J.; Hymel, T. M.; Cui, Y. Electrochemical Tuning of MoS_2 Nanoparticles on Three-Dimensional Substrate for Efficient Hydrogen Evolution. *ACS Nano* **2014**, *8* (5), 4940–4947.

(15) Tsai, C.; Li, H.; Park, S.; Park, J.; Han, H. S.; Nørskov, J. K.; Zheng, X.; Abild-Pedersen, F. Electrochemical Generation of Sulfur Vacancies in the Basal Plane of MoS_2 for Hydrogen Evolution. *Nat. Commun.* **2017**, *8*, 15113.

(16) Deng, J.; Li, H.; Xiao, J.; Tu, Y.; Deng, D.; Yang, H.; Tian, H.; Li, J.; Ren, P.; Bao, X. Triggering the Electrocatalytic Hydrogen Evolution Activity of the Inert Two-Dimensional MoS_2 Surface via Single-Atom Metal Doping. *Energy Environ. Sci.* **2015**, *8* (5), 1594–1601.

(17) Shi, Y.; Zhou, Y.; Yang, D.-R.; Xu, W.-X.; Wang, C.; Wang, F.-B.; Xu, J.-J.; Xia, X.-H.; Chen, H.-Y. Energy Level Engineering of MoS_2 by Transition-Metal Doping for Accelerating Hydrogen Evolution Reaction. *J. Am. Chem. Soc.* **2017**, *139* (43), 15479–15485.

(18) Benson, E. E.; Zhang, H.; Schuman, S. A.; Nanayakkara, S. U.; Bronstein, N. D.; Ferrere, S.; Blackburn, J. L.; Miller, E. M. Balancing the Hydrogen Evolution Reaction, Surface Energetics, and Stability of Metallic MoS_2 Nanosheets via Covalent Functionalization. *J. Am. Chem. Soc.* **2018**, *140* (1), 441–450.

(19) Wang, J.; Yan, M.; Zhao, K.; Liao, X.; Wang, P.; Pan, X.; Yang, W.; Mai, L. Field Effect Enhanced Hydrogen Evolution Reaction of MoS_2 Nanosheets. *Adv. Mater.* **2017**, *29* (7), 1604464-n/a.

(20) Yan, M.; Pan, X.; Wang, P.; Chen, F.; He, L.; Jiang, G.; Wang, J.; Liu, J. Z.; Xu, X.; Liao, X.; Yang, J.; Mai, L. Field-Effect Tuned Adsorption Dynamics of VSe_2 Nanosheets for Enhanced Hydrogen Evolution Reaction. *Nano Lett.* **2017**, *17* (7), 4109–4115.

(21) Yoo, Y.; Degregorio, Z. P.; Johns, J. E. Seed Crystal Homogeneity Controls Lateral and Vertical Heteroepitaxy of Monolayer MoS_2 and WS_2. *J. Am. Chem. Soc.* **2015**, *137* (45), 14281–14287.

(22) Yu, Y.; Li, C.; Liu, Y.; Su, L.; Zhang, Y.; Cao, L. Controlled Scalable Synthesis of Uniform, High-Quality Monolayer and Few-Layer MoS_2 Films. *Sci. Rep.* **2013**, *3*, 1866.

(23) Yu, Y.; Huang, S.-Y.; Li, Y.; Steinmann, S. N.; Yang, W.; Cao, L. Layer-Dependent Electrocatalysis of MoS_2 for Hydrogen Evolution. *Nano Lett.* **2014**, *14* (2), 553–558.

(24) Li, G.; Zhang, D.; Yu, Y.; Huang, S.; Yang, W.; Cao, L. Activating MoS_2 for PH-Universal Hydrogen Evolution Catalysis. *J. Am. Chem. Soc.* **2017**, *139* (45), 16194–16200.

(25) Seh, Z. W.; Kibsgaard, J.; Dickens, C. F.; Chorkendorff, I.; Nørskov, J. K.; Jaramillo, T. F. Combining Theory and Experiment in Electrocatalysis: Insights into Materials Design. *Science (80-.).* **2017**, *355* (6321), eaad4998.

(26) Shinagawa, T.; Garcia-Esparza, A. T.; Takanabe, K. Insight on Tafel Slopes from a Microkinetic Analysis of Aqueous Electrocatalysis for Energy Conversion. *Sci. Rep.* **2015**, *5* (September), 1–21.

(27) Parsons, R. The Rate of Electrolytic Hydrogen Evolution and the Heat of Adsorption of Hydrogen. *Trans. Faraday Soc.* **1958**, *54*, 1053.

(28) Nørskov, J. K.; Bligaard, T.; Logadottir, A.; Kitchin, J. R.; Chen, J. G.; Pandelov, S.; Stimming, U. Trends in the Exchange Current for Hydrogen Evolution. *J. Electrochem. Soc.* **2005**, *152* (3), J23.

(29) Trasatti, S. Work Function, Electronegativity, and Electrochemical Behaviour of Metals: III. Electrolytic Hydrogen Evolution in Acid Solutions. *J. Electroanal. Chem. Interfacial Electrochem.* **1972**, *39* (1), 163–184.

(30) Sheng, W.; Myint, M.; Chen, J. G.; Yan, Y. Correlating the Hydrogen Evolution Reaction Activity in Alkaline Electrolytes with the Hydrogen Binding Energy on Monometallic Surfaces. *Energy Environ. Sci.* **2013**, *6* (5), 1509–1512.

(31) Zhang, Y.; Kolmakov, A.; Chretien, S.; Metiu, H.; Moskovits, M. Control of Catalytic Reactions at the Surface of a Metal Oxide Nanowire by Manipulating Electron Density Inside It. *Nano Lett.* **2004**, *4* (3), 403–407.

(32) Baker, L. R.; Hervier, A.; Kennedy, G.; Somorjai, G. A. Solid-State Charge-Based Device for Control of Catalytic Carbon Monoxide Oxidation on Platinum Nanofilms Using External Bias and Light. *Nano Lett.* **2012**, *12* (5), 2554–2558.

Table of Contents